Geomechanics and Engineering, *Vol. 12, No. 6 (2017) 983-1001*
DOI: https://doi.org/10.12989/gae.2017.12.6.983

Determination of active failure surface geometry for cohesionless backfills

Adlen Altunbas [1a], Behzad Soltanbeigi [2b] and Ozer Cinicioglu [*3]

[1] *Department of Civil Engineering, Beykent University, Istanbul 34398, Turkey*
[2] *Institute for Infrastructure & Environment, School of Engineering, University of Edinburgh, UK*
[3] *Department of Civil Engineering, Bogazici University, Bebek, Istanbul 34342, Turkey*

(*Received July 21, 2016, Revised December 27, 2016, Accepted January 23, 2017*)

Abstract. The extent by which economy and safety concerns can be addressed in earth retaining structure design depends on the accuracy of the assumed failure surface. Accordingly, this study attempts to investigate and quantify mechanical backfill properties that control failure surface geometry of cohesionless backfills at the active state for translational mode of wall movements. For this purpose, a small scale 1 g physical model study was conducted. The experimental setup simulated the conditions of a backfill behind a laterally translating vertical retaining wall in plane strain conditions. To monitor the influence of dilative behavior on failure surface geometry, model tests were conducted on backfills with different densities corresponding to different dilation angles. Failure surface geometries were identified using particle image velocimetry (PIV) method. Friction and dilation angles of the backfill are calculated as functions of failure stress state and relative density of the backfill using a well-known empirical equation, making it possible to quantify the influence of dilation angle on failure surface geometry. As a result, an empirical equation is proposed to predict active failure surface geometry for cohesionless backfills based on peak dilatancy angle. It is shown that the failure surface geometries calculated using the proposed equation are in good agreement with the identified failure surfaces.

Keywords: active state; particle image velocimetry (PIV); dilatancy; retaining wall; physical modelling

1. Introduction

In practice, classical theories proposed by Coulomb (1776) and Rankine (1857) are conventionally used in the design of geotechnical structures that retain soil. However, the fundamental assumption of both theories is that the shear plane formed in the backfill at the ultimate state is a straight line, the slope of which is only a function of the internal friction angle of the backfill. But, experimental evidences (Terzaghi 1936, 1943, Tsagareli 1965, Fang and Ishibashi 1986, Toyosawa *et al*. 2006) and results of numerical modelling studies (Goel and Patra 2008, Benmeddour *et al*. 2012, Shukla and Bathurst 2012, Ismeik and Shaqour 2015, Keshavarz and Pooresmaeil 2016) suggest that backfill failure plane is nonlinear. This difference between

*Corresponding author, Associate Professor, E-mail: ozer.cinicioglu@boun.edu.tr
[a] Ph.D., E-mail: Adlenaltunbas@beykent.edu.tr
[b] Ph.D. Candidate, E-mail: b.soltanbeigi@ed.ac.uk

Copyright © 2017 Techno-Press, Ltd.
http://www.techno-press.org/?journal=gae&subpage=7 ISSN: 2005-307X (Print), 2092-6219 (Online)

classical theories and real behavior results in computed earth pressures that deviate from actual values (Song *et al*. 2015). Many researchers have made assumptions regarding the geometry of failure surfaces (Bang 1985, Hazarika and Matsuzawa 1996, Paik and Salgado 2003, Wang 2000). Terzaghi (1936, 1943), suggested a curvilinear failure surface for walls with rough surfaces by conducting scaled model tests. On the other hand, Caquot and Kerisel (1948) theoretically assumed log spiral shape for the failure slip. Later, Tsagareli (1965) experimentally investigated model walls that translate without rotation and proposed curvilinear failure surfaces that can be mathematically defined with a power function. Spangler and Handy (1982) agreeing with Tsagareli on the curvilinear nature of failure surfaces, proposed a parabolic function for their quantification. Toyosawa *et al*. (2006) conducted centrifuge model tests using a movable earth support apparatus, investigating the influence of mode of wall movement on the geometry of failure surfaces. The results of their study suggested that different modes of wall movements lead to different failure surface geometries. Benmeddour *et al*. (2012) numerically examined the influence of the presence of a slope on the backfill soil and concluded that the shape of the failure surface is influenced by the location of the slope toe.

Even though there is no consensus over the general shape of the active failure plane, it is an established fact that its geometry is affected by the properties of the particles, density of the assembly, the imposed stress state and by the mode of wall movement (Yoshimoto *et al*. 2006). Ignoring mode of wall movement, the parameter that embodies both the mechanical properties of the backfill and the influence of the imposed stress state is dilatancy. Several researchers attempted to account for the dilatancy effect by considering the mechanism of arching (Spangler and Handy 1982, Fang and Ishibashi 1986, Goel and Patra 2008, Nadukuru and Michalowski 2012, Sadrekarimi and Damavandinejad 2013), but arching is a complex mechanism which is practically difficult to quantify. Thus, the main purposes in this study are to investigate the effect of dilatancy on the geometry of failure plane in plane strain condition and also to link dilatancy angle to the failure surface geometry. To understand the influence of dilatancy on failure surface geometry, influence of the mode of wall movement is ignored in this study and only translation type of movement is considered. This is achieved by conducting small scale retaining wall model tests. The dilatancy angles of the backfill soils in these tests are calculated as functions of backfill density and failure stress state using the equation proposed by Bolton (1986).Stresses within the backfill at the instance of failure are measured via the soil pressure transducers mounted on the model wall. At the same time, geometries of the corresponding failure surfaces are obtained using particle image velocimetry (PIV) method. This way, it becomes possible to investigate the relationship between dilatancy angle and failure surface geometry. Finally, obtained results are used to propose a new method for calculating the shapes of active failure surfaces as functions of backfill properties.

2. The small scale retaining wall model

In the present study, in order to investigate the dependency of failure surface geometry on dilatant properties of granular assemblies, 1 g small scale retaining wall model tests were conducted. The backfill soils in these tests were prepared with different relative densities (I_D) to achieve different dilatancy angles. Physical model set-up used for this purpose consists of a testing box, a model retaining wall that is capable of translating laterally, a sand pluviation system, a storage tank, a crane, and a data acquisition system, as shown in Fig. 1(a). The distance between

the model wall and the rear wall is equal to 140 cm. Moreover, the testing box is 60 cm in depth, and 50 cm in width, as presented in Figs. 1(b) and (c). Sides of the testing box are made of 20 mm thick Plexiglas allowing the observation and monitoring of soil deformations, as shown in Fig. 1(a). As a result, photographic images of the backfill at different stages of wall deformation can be captured for later analysis. Captured images are analyzed using particle image velocimetry (PIV) method for identifying the geometry of failure surfaces. The model retaining wall is an aluminumplate which is rectangular in cross-section. The height and width of the model wall are 35 cm and 50 cm, respectively. In order to minimize the adverse effects of the rigid boundary at the bottom, the moving plate that simulates the vertical retaining wall is located 15 cm above the bottom of the test box. The model wall is capable of translating laterally either towards or away from the retained backfill. These tests correspond to passive and active failure conditions at the ultimate states, respectively.

The horizontal translation of the wall is provided by an electrical motor-actuator system. The displacements of the model wall are measured by an electronic ruler. Motor displacement steps also provide the means for validating electronic ruler measurements. Five sensitive miniature pressure transducers are mounted along the vertical axis of the retaining wall model for monitoring the variations of lateral earth pressures along the face of the wall, see Fig. 1(d). Furthermore, two miniature pressure transducers were buried in the backfill during the model preparation stage of each test to verify the vertical effective stress calculations based on measured soil densities, see Figs. 1(b) and (c). Data were collected via a multi-channel data logger system which is capable of handling an aggregate data collection rate of 400 kHz, with a maximum per channel sample rate of up to 500 Hz.

(a) Photograph

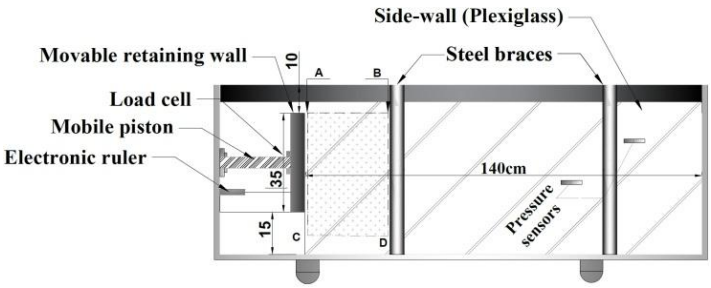

(b) Schematic verticalcross-section

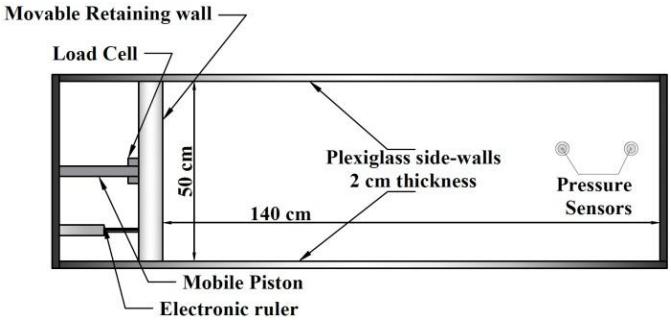

(c) Schematic plan view

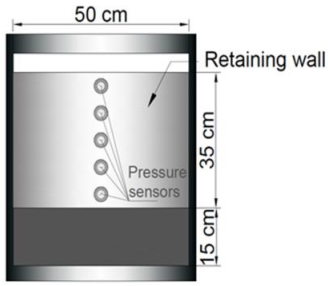

(d) Location of sensors on the wall

Fig. 1 Retaining wall model set-up

3. Calculation of backfill dilatancy in model tests

This paper attempts to investigate the influence of dilatancy on the geometry of active slip surfaces. Theoretically, the influence of dilatant behavior on shear planes is acknowledged (Salençon 1977, Chen and Liu 1990, Atkinson 1981); however, there are no experimental studies that attempt to monitor it for soil bodies except during element tests, such as plane strain and triaxial tests. The underlying reason for this absence is the difficulty associated with the calculation of dilatancy angle from soil properties. Dilatancy angle, which is also referred to as rate of dilation, varies throughout shearing tests with shear strain up to the critical state. Similar to the case of mobilized friction angle, maximum value of dilatancy is measured at the instance of shear failure in granular bodies. Maximum value of dilatancy, referred to as peak dilatancy, correlates well with friction angle and deformation. That is why in this study the focus is on peak dilatancy angle (ψ_p). For this purposethe well-known equation proposed by Bolton (1986), which allows the computation of peak dilatancy angle from backfill density and stress state at failure, is usedin the present investigation. Bolton (1986) equation yields peak dilatancy angle (ψ_p) in degrees as a function of relative density (I_D) and mean effective stress at failure (p'_f)

$$\psi_p = \frac{A_\psi}{r} I_R = \frac{A_\psi}{r}\left[I_D \left(Q - ln \frac{100 p'_f}{p_a} \right) - R \right] \tag{1}$$

Here, Q, R and r are empirical line-fitting parameters that depend on inherent soil characteristics; and p_a is the atmospheric pressure. The value of the constant A_ψ is 3 under axisymmetric conditions and 5 under plane strain conditions (Bolton 1986). Relative density (I_D) varies between 0 and 1. The values of the line-fitting parameters Q and R that are suitable for the testing sand are obtained through triaxial testing. The results obtained in the triaxial tests confirmed the findings of Chakraborty and Salgado (2010) regarding the influence of initial confining stress (p'_i) of the soil on the value of Q. Chakraborty and Salgado (2010) examined the results of numerous triaxial and plane strain tests and reported that the value of the parameter Q depends on the magnitude of initial confining stress (p'_i) of the soil. Accordingly, they proposed that the magnitude of Q can be calculated with an equation of the form given in Eq. (2)

$$Q = \eta + \beta ln p'_i \tag{2}$$

Here, β and η are soil-specific line-fitting parameters that are obtained experimentally. Chakraborty and Salgado (2010) showed that Eq. (2) is suitable for stresses that range from very low to intermediate (stress levels prior to the commencement of grain crushing). In this study numerous triaxial tests were conducted with p'_i values that range from 25 kPa to 500 kPa. As a result, soil specific values of the parameters β, η, and R are obtained. The values of the parameters β, η, and R for the testing sand in this study (Akpinar Sand) are 0.4, 7.2, and 1, respectively. Reported experimental studiesin the literature support the fact that, same peak dilatancy angle is measured in plane strain and triaxial tests (Bolton 1986). Additionally, Schanz and Vermeer (1996) stated that by using concepts of superposition it is possible to show that the data from plane strain and triaxial tests yield the same angle of dilatancy at least near and beyond peak. Consequently, it became possible to calculate the peak dilatancy angle of the model backfill, which rendered the investigation of the influence of dilatancy angle on active failure surface

geometry feasible.

Additionally, the value of the line-fitting parameter r can be calculated using Eq. (3) proposed by Bolton (1986)

$$r = \frac{\phi'_p - \phi'_c}{\psi_p} \tag{3}$$

Here, ϕ'_c is the critical state friction angle. A similar relationship was also suggested by Bishop (1971). Eq. (3) can be rearranged to calculate the value of ϕ'_p relevant for axisymmetric conditions using experimentally obtained r and ϕ'_c. Experimental results reported in the literature shows that measured ϕ'_p values in triaxial and plane strain tests slightly differ from each other (Stroud 1971, Lade 1984, Schanz and Vermeer 1996, Hanna 2001). According to Schanz and Vermeer (1996), this discrepancy stems from the fact that ϕ'_p is dependent on density and stress path. Since the stress path under axisymmetric and plane strain conditions differ, measured ϕ'_p values also differ. To account for this fact, ϕ'_p values computed using Eq. (3) is converted into ϕ'_p values that are relevant for plane strain conditions. For this purpose, the method proposed by Hanna (2001) was used. The steps for this conversion method are given in detail in Hanna (2001). Hanna, testing the conversion method on six different sands, reported that a good agreement was obtained between the predicted results using the proposed method and the experimental results. Therefore, in the present study, ϕ'_p values relevant for the model backfill soils are calculated by computing the axisymmetric ϕ'_p using the rearranged version of Eq. (3), and then converting the obtained value to plane strain ϕ'_p using the method proposed by Hanna (2001). As a result, r value, which was experimentally obtained as 0.39 for axisymmetric conditions, is found as 0.66 for plane strain conditions using Hanna (2001) method.Accordingly, plane strain ϕ'_p values can be calculated using ψ_p calculated from Eq. (1), ϕ'_c of the soil and r value specific to plane strain conditions.

Calculations of the magnitudes of ϕ'_p and ψ_p for the backfill soils requires the knowledge of p'_f. The magnitudes of p'_f in model tests are calculated based on the measurements of the pressure transducers at the instance of failure. Since the available transducers measure normal stresses in the vertical direction and the horizontal direction normal to the model wall, normal stresses parallel to the direction of the plexiglas sidewall's normal has to be based on assumption. Since plane strain conditions prevail in the horizontal direction normal to the sidewalls, it is assumed that the normal stresses in this direction correspond to the steady state condition. Therefore, normal stresses in the direction of the sidewall normal are assumed to be equal to the measured lateral earth pressures before any deformation.

4. Identification of failure surface geometry

Physical model studies require measurements of deformations and strains during testing. This is a difficult task considering the problems associated with instrumenting soil models. To overcome this difficulty, researchers developed different visualization tools that allow the deformations and strains to be computed through the test, such as X-rays (Roscoe *et al*. 1963, Tejchman and Wu 1995), coloured layers and markers (Yoshida *et al*. 1994), X-ray-tomography (Desrues *et al*. 1996, Alshibli and Sture 2000), electrical capacitance tomography (Jaworski and Dyakowski 2001, Niedostatkiewicz *et al*. 2009), photogrammetry and stereo-photogrammetry (Butterfield *et al*. 1970, Desrues 1996), particle image velocimetry (PIV) (White *et al*. 2003, Niedostatkiewicz *et al*.

(a) Defining square patches over images (b) Displacement vector calculation

Fig. 2 Determination of displacement vector field

2011, Lesniewska and Wood 2011, Lesniewska *et al*. 2012, Zhuang *et al*. 2013) and X-ray micro-tomography (Lenoir *et al*. 2007).

In this study Particle Image Velocimetry (PIV), also known as Digital Image Correlation (DIC), was used for measuring deformations and strains. PIV, a digital image-based surface displacement measurement technique, provides highly accurate measurements of evolving deformation fields. PIV tracks particle flow by examining the difference between a reference image and a sequence of deformed images. PIV analyses in this study were conducted with GeoPIV-RG, a Matlab based PIV software specifically utilized for geotechnical applications (Stanier *et al*. 2015). Use of GeoPIV-RG requires the selection of the area of interest within the digital image. After several preliminary model tests, the optimum area of interest is selected to include all the possible deformations during an active test. This area is shown as rectangle ABCD in Fig. 1(b). In the vertical direction, the ABCD rectangle always starts 10cm from below the toe of the wall, to capture possible deformations in the bed section, and elongates up to the top of the wall. Whereas, in the horizontal direction, points A and C always have couple of millimeters of overlap with the wall to record the wall displacement (in other words, the area of 450×250 mm is captured with 4400×2450 pixels, of which corresponds to 10pixels per 1mm). The area ABCD is wide enough to cover any possible deformations and extends up to the brace, as seen in Fig. 1. The camera is located at fix distance from the wall, which ensures the highest precision for the captured images. The selected camera is capturing approximately 4 images per second which is enough for monitoring the quasi-static deformations in the backfill. Defined area is then divided into a grid of square patches as shown in Fig. 2(a). These patches are distinguished by their unique pixel intensity variation signatures. Afterwards, GeoPIV-RG algorithm searches the specified zone within the deformed image to find a patch that has maximum similarity to the initial patch signature. The difference between the target patch, measured in pixels, and the reference patch is visualized by the displacement vector as shown in Fig. 2(b). The most important advantage of using PIV in geotechnical problems is that, unlike hydraulics applications, target markers are not required since soil grains have natural textures (White *et al*. 2003). During the tests, images were captured by a digital camera having resolution of 6000 × 4000 pixels. To prevent vibration of the camera during the shooting, a remote controller was used.

5. Backfill properties and sample preparation

The soil used in the present investigation is Akpinar sand which is uniformly graded according to USCS as shown in Fig. 3. A summary of the physical characteristics of the sand is given in

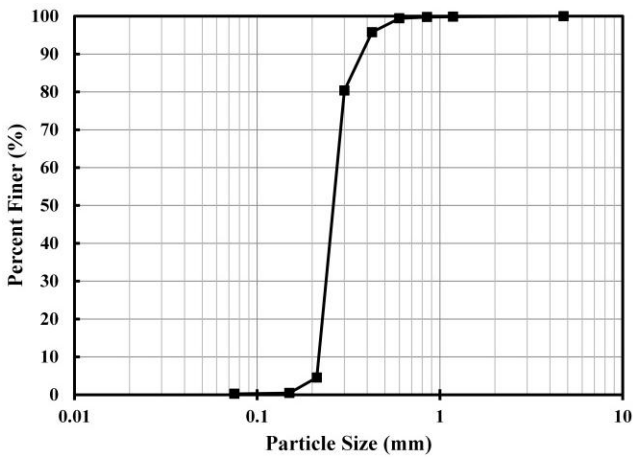

Fig. 3 Gradation curve of Akpinar sand

Table 1 Mechanical properties of Akpinar Sand

Property	Value
Classification	Poorly Graded (SP)
Max. void ratio, (e_{max})	0.87 (ASTM D-4253)
Min. void ratio, (e_{min})	0.58 (ASTM D-4254)
D_{10}	0.22
D_{30}	0.24
D_{50}	0.27
D_{60}	0.28
Uniformity coefficient, (C_u)	1.23
Coefficient of gradation, (C_c)	0.97
Specific gravity, (G_s)	2.63
Average sphericity, (S_{ave})	0.7
Average roundness, (R_{ave})	0.5
Dilatancy effect on friction for axisymmetric conditions, (r_{tx})	0.39
Dilatancy effect on friction for plane strain conditions (r_{ps})	0.66
Critical state friction angle, (ϕ'_c (°))	33

Table 1. Average sphericity and roundness values for Akpinar Sand were obtained based on the grain shape charts proposed by Cho *et al*. (2006). Direct shear tests were conducted to measure the interface friction angle between the model wall and the backfill. In this study, two types of model wall surfaces have been used. For most of the tests, smooth steel surface has been used, and several additional model tests were conducted with sandpaper glued to the wall surface to investigate the influence of wall roughness on the geometry of failure planes. Accordingly, for backfill densities ranging from loosest to densest, wall-backfill interface friction angle was measured to vary between 19° and 23° for smooth surface, and between 35° and 45° for rough surface, respectively. In order to maintain plane strain conditions, low friction transparent high

density polyethylene sheets were used on the plexiglass side walls to minimize friction. Plexiglass used for the side walls of the model tank are 20 mm thick and is reinforced with steel braces to prevent deflection Fig. 1(b).

For investigating the variation of active failure surface geometries, backfill soils were prepared with different dilatant properties. This was achieved by varying the relative densities between tests, since it was not possible to significantly alter the stress states in a 1g test. Accordingly, backfill relative densities (I_D) varied within the range 0.20 to 0.90.

During model preparation, Akpinar sand was placed behind the model retaining wall by dry-pluviation through a hopper. The falling height of sand during pluviation can be adjusted to achieve the desired relative density in the backfill material. Backfill was compacted with a hand-held electrical compactor as necessary, whenever dry-pluviation was not sufficient to achieve target densities. As it was shown in Cinicioglu and Abadkon (2014), overconsolidation ratio (OCR) does not influence dilatant properties. Therefore, compaction induced OCR does not affect the ψ_p values computed using Eq. (1). Density cans (54 mm in diameter, 34 mm in depth) were used to measure the unit weight and to calculate relative density of the backfill during model tests. These cans were placed in a staggered scheme in the vertical direction. At the end of the each experiment, density control cans were extracted carefully and weighed immediately for relative density calculations. The results allowed the confirmation of the homogeneity of the model backfill. Since the variations in the mean effective stress along the depth of the model are insignificant owing to the small size of the model, it is correct to assume that the dilatancy angle is not changing with depth within the backfill. After backfill preparation, model tests were conducted by moving the model wall away from the backfill in a translational mode at a constant speed of 0.5 mm/s. Since there is no rate effect for dry cohesionless sand, selection of the wall translation speed is based on the image-capturing rate of the camera at the defined image quality level. Tests were continued until after active failure state is reached. During the tests, images were captured through the transparent side-walls for every 0.1 mm of wall translation.

6. Failure surface geometry by PIV

GeoPIV-RG provides detailed cumulative shear (ε_s) and volumetric strain (ε_v) maps for every stage of the tests. Through the analyses of these strain maps, shear strain localization can be detected and the evolution of failure surface with wall displacement can be observed. Strain maps are color-coded for visualization of strain magnitude distribution within the model. Following soil mechanics notation, contraction (volume decrease) is considered as positive and dilation (volume increase) as negative. Color-scales of each image were adjusted to achieve highest visual contrast, so that failure surface would be easily distinguishable. A coordinate system with its origin located at the bottom of the model wall is established in order to be able to quantify failure surface geometry. Furthermore, established coordinate system is made non-dimensional by normalizing the axes with model wall height (H_w). Then, unit-independent quantification of the failure surface becomes possible. X and Y coordinates of the points along the failure surface that corresponds to main shear band, are measured as shown in Fig. 4. In this respect, outer edges of failure surfaces are digitized with respect to established coordinate system and quantified for both B (away from the model wall) and H (along the height of the model wall) directions as shown in Figs. 4(a) and (b). Coordinates of all points along the failure plane, horizontal ($B_{1,2,..,n}$) and vertical ($H_{1,2,..,n}$), are measured with respect to the position of the wall prior to any displacement.

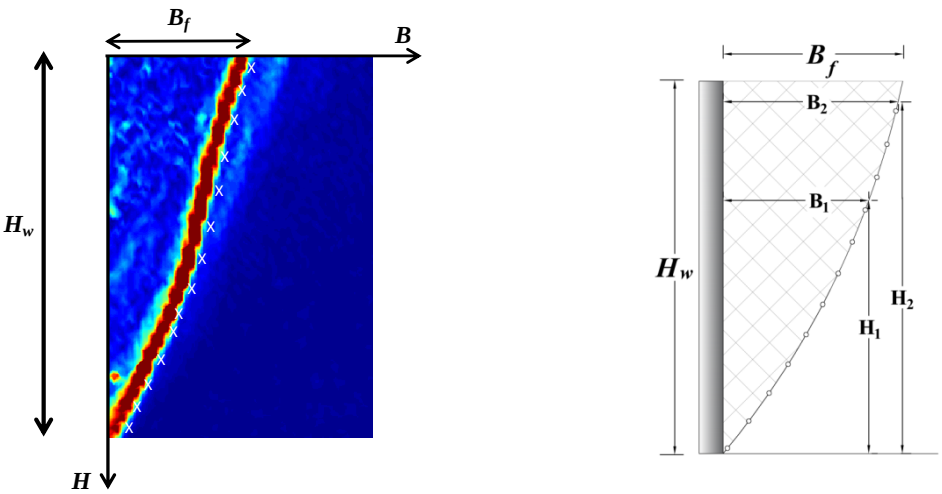

(a) As plotted on the cumulative shear strain map (b) Schematics of proposed coordinate system

Fig. 4 Determination of the failure surface geometry

Using the shear and volumetric strain maps, failure surface can be identified by following the locus of maximum strain points. Evaluating defined failure surfaces, it is observed that greater backfill densities correspond to steeper and more intense shear bands during active wall failures Fig. 5. This is an outcome of higher internal friction (ϕ'_p) and dilatancy (ψ_p) angles associated with greater relative densities. This fact is also supported by Loukidis and Salgado (2011) in their study based on Finite Element Method simulations. Analyzing the consecutive stages of the test from start to finish for models with high dilatancy angles, it has been observed that deformations concentrate to a continuous region even during the initial stages of the test. This region, within which the deformations accumulate gradually during the stages leading up to failure, evolves into failure surface. As soon as failure surface forms, deformations become restricted to the region between the failure surface and the wall as shown in Fig. 6. This area is referred as the failure wedge.

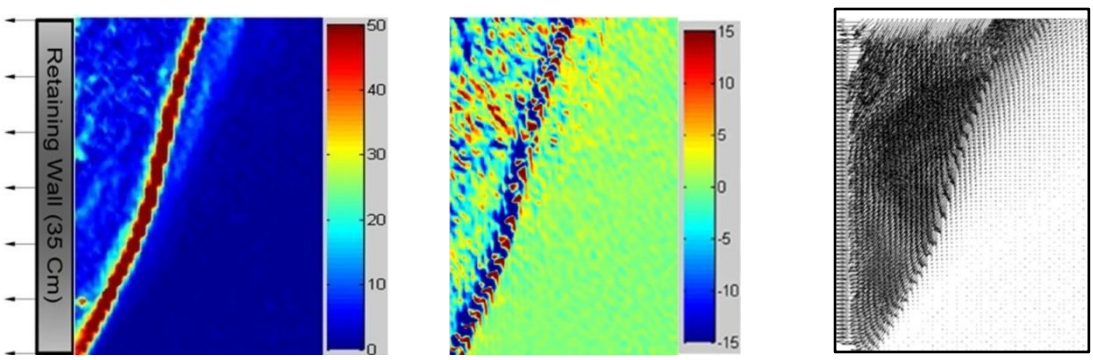

(a) Distribution of shear strains (ε_s) (b) Distribution of volumetric strains (ε_v) (c) Vector field display

Fig. 5 Localization of cumulative strains in initially dense sand

As observed in Figs. 5 and 7, both dilative and contractive deformations can be identified on volumetric strain maps obtained from PIV analyses. Accordingly along the failure band, volumetric deformation is dominantly dilative for dense backfills (Fig. 5(b)) and dominantly contractive for loose backfills (Fig. 7(b)). Evidently, in Fig. 7(b), failure surface is less distinguishable for loose backfills unlike for dense backfills in which failure surfaces are clearly visible. This shows the influence of dilatancy on localization of shear strains in granular materials. Based on this observation, it is possible to propose that the geometry of shear planes can be quantified as functions of dilatancy angle. This proposition has its roots in plasticity theory for geomaterials (Atkinson 1981). A recent study by Niedostatkiewicz *et al*. (2011) also supports the idea that deformation in shear zones is always related to dilatancy.

Based on the results of PIV analyses, general shapes of the failure surfaces were evaluated and plotted as shown in Fig. 8. A new dimensionless coordinate system is established by normalizing the horizontal and vertical dimensions with wall height. The origin of the coordinate system is located at the initial position of the top backfill side corner of the model wall and positive directions are defined as shown in Fig. 8. Results suggest nonlinear active failure surface geometry that links the toe of the rigid retaining wall to the surface of the backfill. Fig. 8 shows the

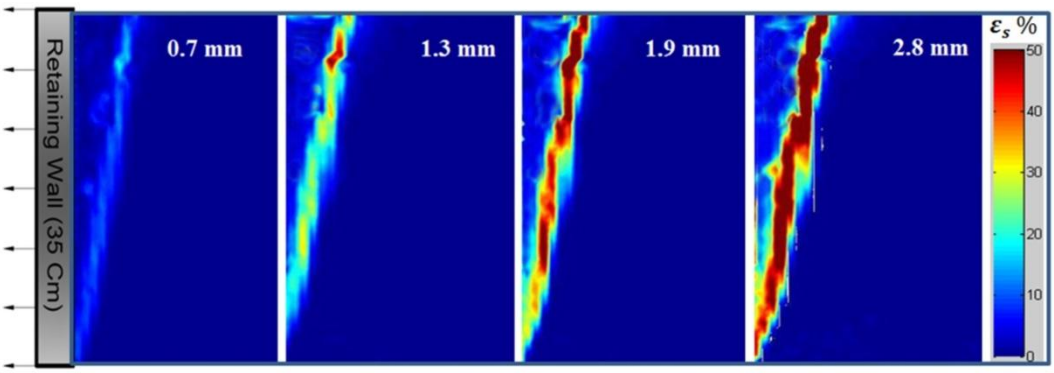

Fig. 6 Shear strain concentration and failure surface evolution with respect to rigid retaining wall movement

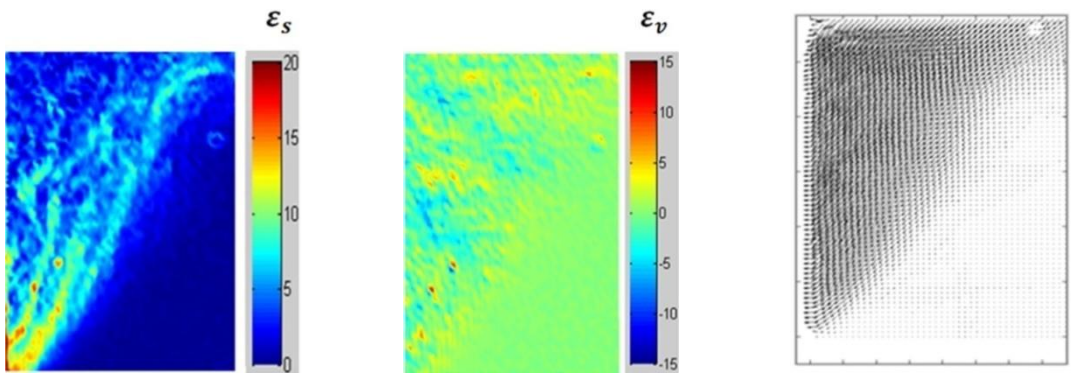

(a) Distribution of shear strains (ε_s) (b) Distribution of volumetric strains (ε_v) (c) Vector field display

Fig. 7 Localization of cumulative strains in initially loose sand

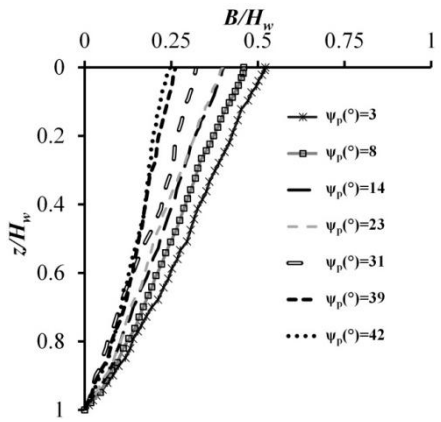

Fig. 8 Geometries of several active failure surfaces obtained from PIV analyses and the corresponding peak dilatancy angles (ψ_p) of the model backfill soils

geometries of the failure surfaces identified from model tests with different backfill properties. Failure surfaces obtained from all model tests are not shown in Fig. 8 for the sake of clarity. Dilatancy angles of the backfills are also reported in Fig. 8. From the analyses of failure surfaces, it is possible to propose that the magnitudes of dilatancy angles influence the shapes of failure surfaces even though the model tests were conducted under 1 g conditions without surcharge and model dilatancy angles were basically controlled by varying the backfill density. Additionally, it should be noted that some tests with close but different ψ_p values have coincident failure surfaces. This conditions stems from the fact that it is very difficult to control small variations in relative densities during model tests. Moreover, identification of the position of the failure surface is more difficult for looser samples since there is greater dispersion of the shear band as shown in Figs. 5 and 7. But the overall trend, higher ψ_p results in more vertical shear bands, is clear from all tests.

7. Determination of failure surface geometry

PIV analyses of the images of model tests at failure revealed that active failure surface is not planar. When the general forms of the failure planes shown in Fig. 8 are examined, parabolic function is identified as the most suitable mathematical function for numerical identification. In literature, the boundary conditions for a parabolic failure surface are defined by Spangler and Handy (1982) and Goel and Patra (2008). According to Spangler and Handy (1982), parabolic equation suitable for defining failure surfaces is shown below

$$z = aB^2 + bB + c \tag{4}$$

where, z defines the vertical coordinate and B defines the horizontal distance from the retaining wall to the failure surface at a particular depth z as depicted in Fig. 4. Using the boundary conditions, constants of the parabolic failure surface can be obtained as follows

$$z = H_w,\ B = 0, \tag{5}$$

$$z = H_w \rightarrow \frac{dz}{dB} = -\tan(\alpha), \tag{6}$$

$$z = 0 \rightarrow B = (a_b) H_w \cot(\alpha), \tag{7}$$

where, a_b is defined as the ratio of B_f to X and α is the inclination of the initial section of the shear band at the toe level. Distance Xis measured horizontally between the wall and the point at which the tangent to the initial portion of the failure surface emerges at the backfill surface, as illustrated in Fig. 9. On the other hand, B_f is the horizontal distance from the wall to the actual point of failure surface emergence at the ground surface Fig. 9. As expected, magnitudes of B_f and X are dependent on the peak dilation angle (ψ_p) of the backfill (Figs. 10(a) and (b)). Moreover, it can be seen that the values of a_b are approximately constant and thus independent of ψ_p, thus an average value is assigned to a_b equal to 0.67 (see Fig. 10(c)).Using the above three boundary conditions, the constants a, b, and c are obtained as follows

$$a = \left[(a_b - 1) / (a_b{}^2 H_w) \right] \tan^2(\alpha), \tag{8a}$$

$$b = -\tan(\alpha), \tag{8b}$$

$$c = H_w \tag{8c}$$

Inserting the constants given in Eq. (8) into Eq. (4), parabolic equation for the active failure surface is obtained as

$$z = \left(\left[(a_b - 1) \Big/ (a_b^2 H_w) \right] \tan^2(\alpha) \right) B^2 - \tan(\alpha) B + H_w \tag{9}$$

The value of α and its correlation with backfill properties is investigated for all the model test results. It is noted that the magnitude of α correlates very well with Eq. (10) as proposed by Vardoulakis (1980)

$$\alpha = \frac{\pi + \phi'_p + \psi_p}{4} \tag{10}$$

Variation of α with ϕ'_p and its comparison with Eq. (10) are shown in Fig. 11. Clearly, experimental data are compatible with Eq. (10).

Then, as a_b is constant as shown in Fig. 10, geometry of the active failure surface can be calculated as a function of soil properties (ϕ'_p and ψ_p) and problem geometry (H_w). Resulting parabolic function is given Eq. (11)

$$z = \left(\left[\frac{(a_b - 1)}{(a_b^2 H_w)} \right] \left(\tan\left(\frac{\pi + \phi'_p + \psi_p}{4} \right) \right)^2 \right) B^2 - \tan\left(\frac{\pi + \phi'_p + \psi_p}{4} \right) B + H_w \tag{11}$$

Accuracy of Eq. (11) in predicting active failure planes is examined by comparing their results

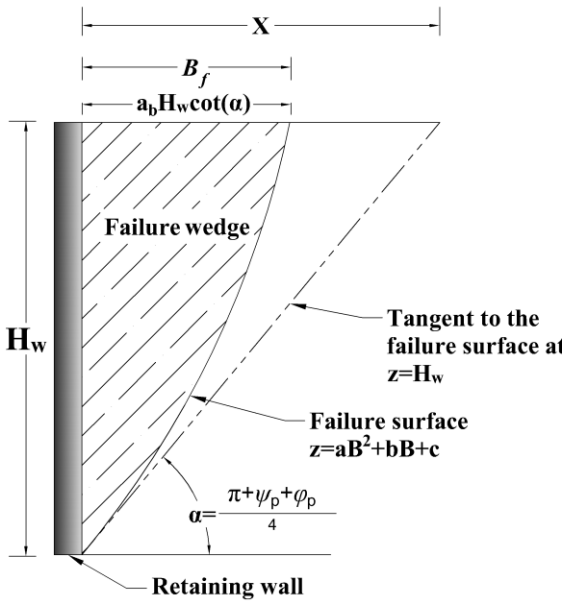

Fig. 9 Shape of the assumed parabolic failure surface and the depiction of the geometrical ratio a_b

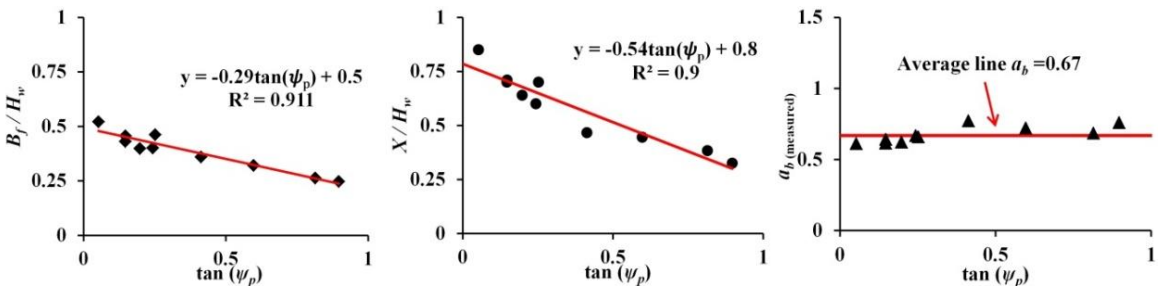

(a) (b) (c)

Fig. 10 Influence of dilatancy angle of the backfill on experimentally measured values for (a) B_f; (b) X; (c) a_b

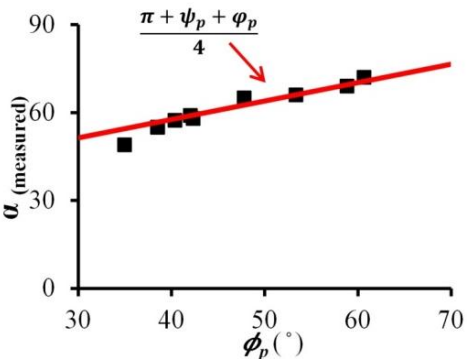

Fig. 11 Variation of α with ϕ_p as obtained from model test results

with the actual failure surfaces obtained by PIV analyses of the physical model tests. It should be noted that ψ_p used in Eq. 11 is calculated using the magnitudes of I_D and p_f' corresponding to the midheight level of the retaining wall. The value of a_b is kept constant at 0.67 for all the calculations.For purposes of comparison, classical planar slip surfaces are also plotted in Fig. 12 as extensions of the initial linear portions of identified failure planes. Additionally, failure surface geometries, as defined by Tsagareli (1965), are included in Fig. 12 for comparison. Results in Fig. 12 show that shapes of the measured failure surfaces and shapes of the predicted failure surfaces using Eq. (11) approximately overlap from toe to the top of backfill. Also, it is observed that the

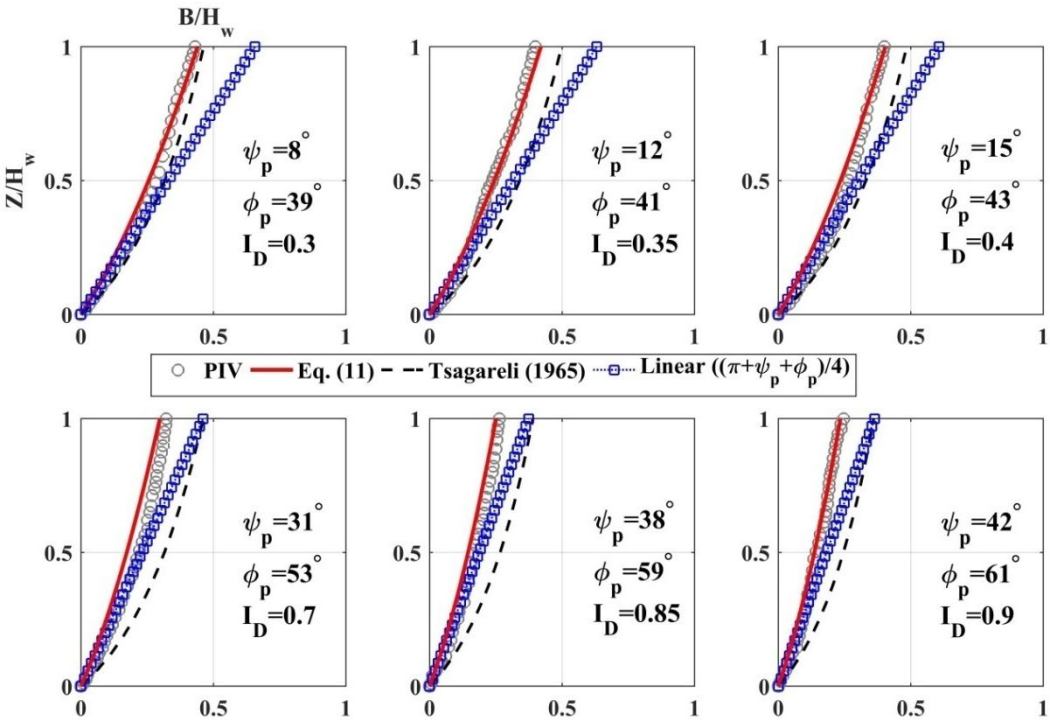

Fig. 12 Comparison between plots of estimated and experimentally visualized failure surfaces with data obtained from literature on normalized coordination system

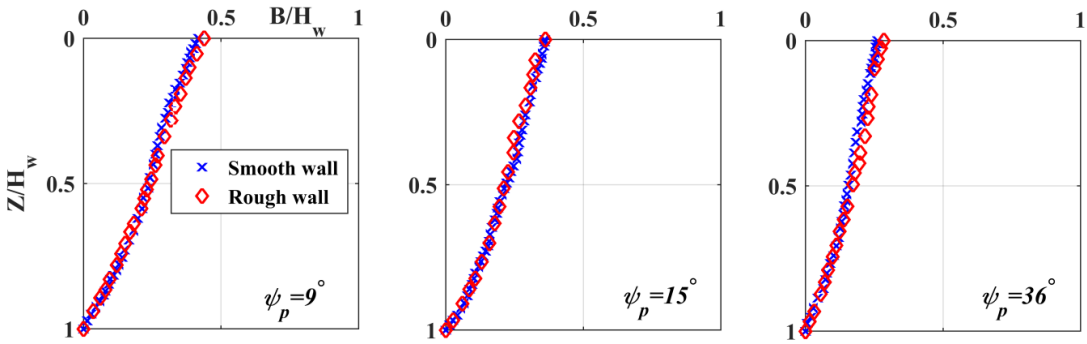

Fig. 13 Influence of wall roughness on failure surface geometry for backfills with different densities

differences are significant between classical method and predicted results, especially for models with denser backfills.

8. Influence of wall-backfill interface friction angle on the geometry of failure surfaces

In order to observe the influence of interface friction angle between the wall and backfill (δ), some of the model tests were repeated with a different wall roughness. To create a rougher wall surface, sandpaper was glued to the face of the wall. The angles of friction between the sandpaper and the backfill were determined by conducting direct shear box tests. According to the results, sandpaper-backfill friction angles varied between 35° and 45° depending on backfill density.

The results of the tests are shown in Fig. 13. Based on the results, it is clearly seen that the changes in the geometries of the slip planes as a result of the variations in wall-backfill interface friction angles (δ) are practically insignificant for active mode of failure states. Therefore, it is stated that effect of wall friction on the shape of the slip surface is small and can be ignored at active failure state as suggested by Craig (2004).

9. Discussion

Dependency of the shape of failure surface on ϕ'_p and ψ_p, as in the case of Eq. (11), is expected since the influences of ϕ'_p and ψ_p have been considered theoretically in soil plasticity (Atkinson 1981, Bolton 1986, Chen and Liu 1990, Salençon 1997). Since dilatant behavior results in a deformation component that is directed out of the plane of shearing, and the initial direction of the shear plane is dependent on ϕ'_p of the soil in soil plasticity theory, geometries of failure planes for frictional soils are controlled by strength and dilatant properties. However, this phenomenon has been dealt with only in theory since it is difficult to measure or calculate dilatancy angles of granular materials that constitute large masses; only dilatancy angles of soil samples can be measured. As a result, geotechnical modelling studies that quantitatively consider dilatancy effects are almost non-existent.

The problems associated with the measurement of ψ_p are overcome in this study by using the equation proposed by Bolton (1986). Using the measured values of I_D and p'_f in Eq. (1), magnitudes of ψ_p are calculated for model backfills. Combining dilatancy calculations with the image processing techniques, it is now possible to examine the influence of dilatant behavior on deforming granular bodies. Consequently, this study investigates and quantifies the effect of dilatancy on active failure surfaces.

On the other hand, usability of Eq. (11) depends on the possibility of knowing the magnitude of the possible value of ψ_p for the backfill soil under consideration. This requires either testing the soil or using the available equations in literature. If the backfill soil can be tested, it is imperative that the possible stress path that the backfill soil will follow to failure should be simulated. This is necessary as the magnitude of ψ_p is the dependent on stress path. However, if the soil cannot be tested in the laboratory, equations proposed for estimating ψ_p might be used. In this case, there are two options. The first option is to use Eq. (1) used in this study. The advantage of this equation is that it can be used to calculate ψ_p for any stress path using the same soil-specific constants as Eq. (1) is a function of p'_f. Yet the line-fitting parameter Q used in Eq. (1) is a function of the p'_i. Therefore, necessary number of line-fitting parameters to be defined and the necessary number of

strength tests to conduct increases. Additionally, unlike the model tests conducted in this study where failure stresses are measured, in practice it is necessary to be able to estimate the possible magnitude of p_f' beforehand. The alternative to Eq. (1) is the equation proposed by Cinicioglu and Abadkon (2014) (Eq. (12)). Eq. (12) allows the computation of ψ_p as a function of pre-shear soil properties I_D and p_i'.

$$\tan\psi_p = \alpha_\psi \left(\frac{p_i'}{p_a} \right) + m_\psi I_D \tag{12}$$

Here, α_ψ and m_ψ are unit-independent empirical soil constants. The main advantage of this equation is that it is based on soil parameters (I_D and p'_i) obtained prior to any deformation, and not on parameters that correspond to failure states. As a result, Eq. (12) can be used to calculate dilatancy angle directly from the information collected during the preparation of cohesionless backfill. Additionally, the influences of p'_i and $I_D$on ψ_p are uncoupled (Cinicioglu and Abadkon 2014). Thus, theoretically two strength tests at different p'_i-I_D combinations are sufficient to calculate soil-specific constants α_ψ and m_ψ. But it should be emphasized that strength tests that are conducted to obtain α_ψ and m_ψ should simulate the stress path expected in the field. Accordingly, extensional triaxial or plane strain tests should be conducted to obtain α_ψ and m_ψ constants suitable for active failure states. Calculated ψ_p values are valid both under axisymmetric and plane-strain conditions. However, to calculate the ϕ'_p value appropriate for plane-strain conditions using Eq. (3) as in the case of this study, it is necessary to use Hanna (2001) method to obtain r value specific for plane-strain conditions if it is not possible to conduct plane-strain tests. Consequently, it is also possible to use the proposed equations in practical applications. Since a_b is a constant independent of wall height and roughness, the results are generally applicable to active state during wall translation for small size granular materials. However, possible influences of different modes of wall movements on active failure surface geometries and a_b-$\tan\psi_p$ relationships should be investigated.

10. Conclusions

This study attempts to quantify active failure surface geometry using the results obtained from small scale physical model tests. For this purpose, a small scale retaining wall model has been constructed. Several model tests were conducted at 1 g until active failure. Images from the tests were analyzed using PIV method and the resulting failure surfaces were identified. Following the proposition of soil plasticity theory that the shapes of failure surfaces in frictional materials are dependent on the dilatant properties, influence of peak dilatancy angle on active shear planes is investigated. Analyzing the results, it is noticed that there is a clear and direct correlation between the calculated dilatancy angles and general characteristics of the active failure surfaces. Additionally, model test results suggest that the geometries of active failure surfaces can be quantified using a parabolic function, as previously proposed by Spangler and Handy (1982). Accordingly, a parabolic function that uses ϕ'_p, ψ_p, and wall height as inputs is defined for calculating the shapes of the active failure surfaces for problems in which the backfill is horizontal and the wall moves in horizontal translation mode. A number of the model tests were repeated only by changing wall roughness and it was shown that wall roughness does not influence the geometry of active failure surfaces. The results also showed that the initial inclination of active failure

surfaces can best be estimated as $(\pi + \phi_p + \psi_p)/4$ as proposed by Vardoulakis (1980). Additionally, normalized horizontal distance of the point of emergence of the failure plane on ground surface (a_b) to the wall is practically constant. Finally, calculated failure surfaces using the proposed equation are compared with both the experimentally visualized and planar slip surfaces and the results are discussed.

Acknowledgments

Authors would like to thank the Scientific and Technological Research Council of Turkey (TUBITAK Project 110M595) for providing financial support.

References

Alshibli, K.A. and Sture, S. (2000), "Shear band formation in plane strain experiments of sand", *J. Geotech. Geoenviron. Eng.*, **126**(6), 495-503.

Atkinson, J.H. (1981), *Foundations and Slopes*, McGraw-Hill, London, UK.

Bang, S. (1985), "Active earth pressure behind retaining walls", *J. Geotech. Eng.*, **111**(3), 407-412.

Benmeddour, D., Mellas, M., Frank, R. and Mabrouki, A. (2012), "Numerical study of passive and active earth pressures of sands", *Comput. Geotech.*, **40**, 34-44.

Bishop, A.W. (1971), "Shear strength parameters for undisturbed and remoulded soil specimens", *Proceedings of the Roscoe Memorial Symposium*, Cambridge University, Cambridge, MA, USA, pp. 3-58.

Bolton, M.D. (1986), "The strength and dilatancy of sands", *Geotechnique*, **36**(1), 65-78.

Butterfield, R., Harkness, R.M. and Andrews, K.Z. (1970), "A stero-photogrammetric method for measuring displacement fields", *Géotechnique*, **20**(3), 308-314.

Caquot, A.I. and Kérisel, J.L. (1948), *Tables for the Calculation of Passive Pressure, Active Pressure and Bearing Capacity of Foundations*, Gauthier-Villars.

Chakraborty, T. and Salgado, R. (2010), "Dilatancy and shear strength of sand at low confining pressures", *J. Geotech. Geoenviron. Eng.*, **136**(3), 527-532.

Chen, W.-F. and Liu, X.L. (1990), *Limit Analysis in Soil Mechanics*, Elsevier, 52 p.

Cho, G.-C., Dodds, J. and Santamarina, J.C. (2006), "Particle shape effects on packing density, stiffness, and strength: Natural and crushed sands", *J. Geotech. Geoenviron. Eng.*, **132**(5), 591-602.

Cinicioglu, O. and Abadkon, A. (2014), "Dilatancy and friction angles based on in-situ soil conditions", *J. Geotech. Geoenviron. Eng.*, **141**(4), 6014019.

Coulomb, C.A. (1776), "An attempt to apply the rules of maxima and minima to several problems of stability related to architecture", *Mem. Acad. Roy. des Sciences*, **7**, 343-382.

Craig, R.F. (2004), *Craig's Soil Mechanics*, CRC Press.

Desrues, J., Chambon, R., Mokni, M. and Mazerolle, F. (1996), "Void ratio evolution inside shear bands in triaxial sand specimens studied by computed tomography", *Géotechnique*, **46**(3), 529-546.

Fang, Y.-S. and Ishibashi, I. (1986), "Static earth pressures with various wall movements", *J. Geotech. Eng.*, **112**(3), 317-333.

Goel, S. and Patra, N.R. (2008), "Effect of arching on active earth pressure for rigid retaining walls considering translation mode", *Int. J. Geomech.*, **8**(2), 123-133.

Hanna, A. (2001), "Determination of plane-strain shear strength of sand from the results of triaxial tests", *Can. Geotech. J*, **38**(6), 1231-1240.

Hazarika, H. and Matsuzawa, H. (1996), "Wall displacement modes dependent active earth pressure analyses using smeared shear band method with two bands", *Comput. Geotech.*, **19**(3), 193-219.

Ismeik, M. and Shaqour, F. (2015), "Seismic lateral earth pressure analysis of retaining walls", *Geomech. Eng., Int. J.*, **8**(4), 523-540.

Jaworski, A.J. and Dyakowski, T. (2001), "Application of electrical capacitance tomography for measurement of gas-solids flow characteristics in a pneumatic conveying system", *Measure. Sci. Technol.*, **12**(8), 1109.

Keshavarz, A. and Pooresmaeil, Z. (2016), "Static and seismic active lateral earth pressure coefficients for *c-ϕ* soils", *Geomech. Eng., Int. J.*, **10**(5), 657-676.

Lade, P.V. (1984), *Failure Criterion for Frictional Materials*, Wiley and Sons, London, UK.

Lenoir, N., Bornert, M., Desrues, J., Bésuelle, P. and Viggiani, G. (2007), "Volumetric digital image correlation applied to X-ray microtomography images from triaxial compression tests on argillaceous rock", *Strain*, **43**(3), 193-205.

Leśniewska, D. and Wood, D.M. (2011), "Photoelastic and photographic study of a granular material", *Géotechnique*, **61**(7), 605-611.

Leśniewska, D., Niedostatkiewicz, M. and Tejchman, J. (2012), "Experimental study on shear localization in granular materials within combined strain and stress field", *Strain*, **48**(5), 430-444.

Loukidis, D. and Salgado, R. (2011), "Active pressure on gravity walls supporting purely frictional soils", *Can. Geotech. J.*, **49**(1), 78-97.

Nadukuru, S.S. and Michalowski, R.L. (2012), "Arching in distribution of active load on retaining walls", *J. Geotech. Geoenviron. Eng.*, **138**(5), 575-584.

Niedostatkiewicz, M., Tejchman, J., Chaniecki, Z. and Grudzień, K. (2009), "Determination of bulk solid concentration changes during granular flow in a model silo with ECT sensors", *Chem. Eng. Sci.*, **64**(1), 20-30.

Niedostatkiewicz, M., Lesniewska, D. and Tejchman, J. (2011), "Experimental analysis of shear zone patterns in cohesionless for earth pressure problems using particle image velocimetry", *Strain*, **47**(s2), 218-231.

Paik, K.H. and Salgado, R. (2003), "Estimation of active earth pressure against rigid retaining walls considering arching effects", *Geotechnique*, **53**(7), 643-653.

Rankine, W.J.M. (1857), "On the stability of loose earth", *Philosoph. Trans. Royal Soc. London*, **147**, 9-27.

Roscoe, K.H., Arthur, J.R.F and James, R.G. (1963), *Determination of Strains in Soils by X-Ray Method*, Defense Technical Information Center.

Sadrekarimi, A. and Damavandinejad Monfared, S. (2013), "Numerical investigation of the mobilization of active earth pressure on retaining walls", *Proceedings of 18th International Conference on Soil Mechanics and Geotechnical Engineering*, Paris, France, September.

Salençon, J. (1977), *Application of the Theory of Plasticity in Soil Mechanics*, John Wiley and Sons.

Schanz, T. and Vermeer, P.A. (1996), "Angles of friction and dilatancy of sand", *Geotechnique*, **46**(1), 145-152.

Shukla, S.K. and Bathurst, R.J. (2012), "An analytical expression for the dynamic active thrust from *c-φ* soil backfill on retaining walls with wall friction and adhesion", *Geomech. Eng., Int. J.*, **4**(3), 209-218.

Song, L., Zheng, D.F., Nian, T.K., Liu, B. and Yin, P. (2015), "Coefficient charts for active earth pressures under combined loadings", *Geomech. Eng., Int. J.*, **8**(3), 461-476.

Spangler, M.G. and Handy, R.L. (1982), *Soil Engineering Harper and Row*, New York, NY, USA.

Stanier, S.A., Blaber, J., Take, W.A. and White, D.J. (2015), "Improved image-based deformation measurement for geotechnical applications", *Can. Geotech. J.*, **53**(5), 727-739.

Stroud, M.A. (1971), *The Behaviour of Sand at Low Stress Levels in Simple-Shear Apparatus*, University of Cambridge, UK.

Tejchman, J. and Wu, W. (1995), "Experimental and Numerical Study of Sand–Steel Interfaces", *Int. J. Numer. Anal. Method. Geomech.*, **19**(8), 513-536.

Terzaghi, K. (1936), "A fundamental fallacy in earth pressure computations", *Boston Society Civil Engineers Journal*.

Terzaghi, K. (1943), *Theoretical Soil Mechanics*, Wiley.

Toyosawa, Y.I., Tamrakar, S.B. and Suemasa, N. (2006), "Redistribution of active earth pressures using movable earth support apparatus in centrifuge", *Phys. Model. Geotech.– 6th ICPMG*, pp. 1113-1118.

Tsagareli, Z.V. (1965), "Experimental investigation of the pressure of a loose medium on retaining walls

with a vertical back face and horizontal backfill surface", *Soil Mech. Found. Eng.*, **2**(4), 197-200.
Vardoulakis, I. (1980), "Shear band inclination and shear modulus of sand in biaxial tests", *Int. J. Numer. Anal. Met. Geomech.*, **4**(2), 103-119.
Wang, Y.-Z. (2000), "Distribution of earth pressure on a retaining wall", *Geotechnique*, **50**(1), 83-88.
White, D.J., Take, W.A. and Bolton, M.D. (2003), "Soil deformation measurement using Particle Image Velocimetry (PIV) and photogrammetry", *Geotechnique*, **53**(7), 619-631.
Yoshida, T. (1994), "Shear banding in sands observed in plane strain compression", *Proceedings of Symposium on Localization and Bifurcation Theory for Soils and Rocks*, Balkema, pp. 165-179.
Yoshimoto, N., Wu, Y., Hyodo, M. and Nakata, Y. (2016), "Effect of relative density on the shear behaviour of granulated coal ash", *Geomech. Eng., Int. J.*, **10**(2), 207-224.
Zhuang, L., Nakata, Y. and Lee, I.M. (2013), "Localized deformation in sands and glass beads subjected to plane strain compressions", *Geomech. Eng., Int. J.*, **5**(6), 499-517.

CC